



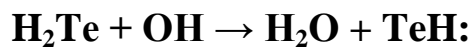
PCCP

The Highly Exothermic Hydrogen Abstraction Reaction $\text{H}_2\text{Te} + \text{OH} \rightarrow \text{H}_2\text{O} + \text{TeH}$: Comparison with Analogous Reactions for H_2Se and H_2S

Journal:	<i>Physical Chemistry Chemical Physics</i>
Manuscript ID	CP-ART-12-2022-005989.R1
Article Type:	Paper
Date Submitted by the Author:	07-Feb-2023
Complete List of Authors:	<p>Tang, Mei; Southwest University of Science and Technology, Li, Guoliang; South China Normal University, School of Chemistry and Environment Guo, Minggang; Baoji University of Arts and Sciences, College of Physics and Optoelectronics Technology Liu, Guilin; Southwest University of Science and Technology Huang, Yuqian; Southwest University of Science and Technology Zeng, Shuqiong; Southwest University of Science and Technology Niu, Zhenwei; Southwest University of Science and Technology Ge, Nina; Southwest University of Science and Technology, Xie, Yaoming; University of Georgia, Center for Computational Quantum Chemistry Schaefer, Henry; University of Georgia, Computational Chemistry</p>

SCHOLARONE™
Manuscripts

The Highly Exothermic Hydrogen Abstraction Reaction



Comparison with Analogous Reactions for H₂Se and H₂S

Mei Tang,^a Guoliang Li,^b Minggang Guo,^c Guilin Liu,^a Yuqian Huang,^a
Shuqiong Zeng,^a Zhenwei Niu,^{a*} Nina Ge,^a Yaoming Xie,^d and Henry F. Schaefer^{d*}

^a*School of Materials and Chemistry, Southwest University of Science and Technology,
Mianyang 621010, China;*

^b*School of Chemistry, South China Normal University, Guangzhou, 510006, China;*

^c*College of Physics and Optoelectronics Technology, Baoji University of Arts and Sciences,
Baoji 721016, China;*

^d*Center for Computational Quantum Chemistry, University of Georgia, Athens, GA
30602, USA.*

E-mail: z.w.niu@swust.edu.cn (Z. N.), ccq@uga.edu (H. F. S.)

Abstract

The "gold standard" CCSD(T) method is adopted along with the correlation consistent basis sets up to aug-cc-pV5Z-PP to study the mechanism of the hydrogen abstraction reaction $\text{H}_2\text{Te} + \text{OH}$. The predicted geometries and vibrational frequencies for reactants and products are in good agreement with the available experimental results. With the ZPVE corrections, the transition state in the favorable pathway of this reaction energetically lies 1.2 kcal/mol below the reactants, which is lower than the analogous relative energies for the $\text{H}_2\text{Se} + \text{OH}$ reaction (-0.7 kcal/mol), the $\text{H}_2\text{S} + \text{OH}$ reaction ($+0.8$ kcal/mol) and the $\text{H}_2\text{O} + \text{OH}$ reaction ($+9.0$ kcal/mol). Accordingly, the exothermic reaction energies for these related reactions are predicted to be 47.8 (H_2Te), 37.7 (H_2Se), 27.1 (H_2S), and 0.0 (H_2O) kcal/mol, respectively. Geometrically, the low-lying reactant complexes for $\text{H}_2\text{Te} + \text{OH}$ and $\text{H}_2\text{Se} + \text{OH}$ are two-center three-electron hemibonded structures, whereas those for $\text{H}_2\text{S} + \text{OH}$ and $\text{H}_2\text{O} + \text{OH}$ are hydrogen-bonded. With ZPVE and spin-orbit coupling corrections, the relative energies for the reactant complex, transition state, product complex, and the products for the $\text{H}_2\text{Te} + \text{OH}$ reaction are estimated to be -13.1 , -1.0 , -52.0 , and -52.6 kcal/mol, respectively. Finally, twenty-eight DFT functionals have been tested systematically to assess their ability in describing the potential energy surface of the $\text{H}_2\text{Te} + \text{OH}$ reaction. The best of these functionals for the corresponding energetics are -9.9 , -1.4 , -46.4 , and -45.4 kcal/mol (MPWB1K), or -13.1 , -2.4 , -57.1 , and -54.6 kcal/mol (M06-2X), respectively.

1. Introduction

Tellurium is the heaviest stable chalcogen, and it exhibits various oxidation states ranging from -2 (H_2Te) to $+6$ (TeO_4^{2-}), just like its close relatives sulfur and selenium. Recently, the valence isoelectronic reactions of H_2X ($\text{X} = \text{O}, \text{S}, \text{and Se}$) with the OH radical, the most common oxidant in the troposphere,^[1] have been studied using the "gold standard" CCSD(T) method.^[2-4] The potential energy surfaces for the three parallel reactions show some variations. For example, the energy of transition state for the $\text{H}_2\text{O} + \text{OH}$ reaction relative to the reactants is high (9.5 kcal/mol), while that for the $\text{H}_2\text{S} + \text{OH}$ reaction is almost zero (0.1 kcal/mol) and that for $\text{H}_2\text{Se} + \text{OH}$ is even lower (-1.7 kcal/mol). Also, the low-lying reactant complex for $\text{H}_2\text{S} + \text{OH}$ and $\text{H}_2\text{O} + \text{OH}$ is a conventional hydrogen-bonded structure, while that for $\text{H}_2\text{Se} + \text{OH}$ is a structure with a two-center three-electron (2c-3e) hemi-bond. In addition, there are two promising pathways for the $\text{H}_2\text{Se} + \text{OH} \rightarrow \text{SeH} + \text{H}_2\text{O}$ reaction, whereas only one pathway was found for the $\text{H}_2\text{O} + \text{OH} \rightarrow \text{OH} + \text{H}_2\text{O}$ and $\text{H}_2\text{S} + \text{OH} \rightarrow \text{SH} + \text{H}_2\text{O}$ reactions.

The above research brings about a growing interest in further study of the analogous reaction for the heavier congener, that is, the $\text{H}_2\text{Te} + \text{OH} \rightarrow \text{TeH} + \text{H}_2\text{O}$ reaction. In fact, tellurium-containing compounds have been applied in the field of biology as antibiotics and anticancer drugs,^[5, 6] and in the field of material science.^[7-12] Hydrogen telluride (H_2Te) is one of the most useful tellurium reagents in synthetic organic chemistry.^[13] H_2Te and its analogs H_2S and H_2Se are well-known precursors for the synthesis of hydrochalcogenides. In 2015, Franke *et al.* synthesized a series of new mono- and dinuclear uranium(IV) hydrochalcogenido complexes via the reaction of H_2E ($\text{E} = \text{S}, \text{Se}, \text{Te}$) with uranium(III).^[14] Kumar and Francisco subsequently pointed out that the nature of heteroatom in H_2X ($\text{X} = \text{O}, \text{S}, \text{Se}, \text{and Te}$) plays a crucial role in determining the reactivity of bimolecular reactions of Criegee intermediates and H_2X .^[15]

Although some H_2Te reactions have been examined,^[14-16] to the best of our knowledge, very little is known about the prototypical $\text{H}_2\text{Te} + \text{OH} \rightarrow \text{TeH} + \text{H}_2\text{O}$ reaction.

It is worth noting that the bonds in H_2Te are so weak that the molecule decomposes spontaneously to Te and H_2 in air already above 0°C , and it will be challenging to measure accurately the rate constant with OH. Thus, a reliable potential energy surface for the title reaction is of significant importance, following our previous studies of the reactions of OH radical with H_2O , H_2S and H_2Se .^[2-4] In the current study, structures, energetics, and vibrational frequencies for stationary points on the $\text{H}_2\text{Te} + \text{OH}$ potential surface are characterized, and these results are compared with the related H_2X ($\text{X} = \text{O}, \text{S}, \text{Se}$) + OH reactions.

2. Theoretical Methods

In this study, the potential energy surface for the $\text{H}_2\text{Te} + \text{OH}$ reaction was explored using the "gold standard" CCSD(T) method, which denotes the coupled-cluster single and double substitution method with a perturbative treatment of triple excitations for systems dominated by a single configuration.^[17-19] The UHF reference was utilized in the CCSD(T) computations for the open-shell systems.

For the hydrogen and oxygen atoms, Dunning's augmented correlation-consistent polarized valence basis sets aug-cc-pVnZ ($n = \text{D}, \text{T}, \text{Q},$ and 5) were used.^[20, 21] For the tellurium atom, we adopted the multiconfiguration Dirac-Hartree-Fock adjusted small-core relativistic pseudopotential (PP) in conjunction with the corresponding augmented correlation-consistent basis sets, i.e., aug-cc-pVnZ-PP ($n = \text{D}, \text{T}, \text{Q},$ and 5).^[22] With the pseudopotential, 28 core electrons ($1s^2 2s^2 2p^6 3s^2 3p^6 3d^{10}$) are embodied in the effective core for the tellurium atom. In the text below, for the sake of brevity, we may abbreviate DZ, TZ, QZ, and 5Z to represent aug-cc-pVnZ ($n = \text{D}, \text{T}, \text{Q},$ and 5) for H and O, as well as aug-cc-pVnZ-PP for Te. The geometry optimizations were conducted with basis sets up to QZ, and the energy profile was refined by performing single-point computation using the larger 5Z basis sets. In this CCSD(T) research, the 1s-like molecular orbital (MO) was frozen for the oxygen atom, while the 4s4p4d-like MOs were frozen for tellurium. To

characterize the nature of all the stationary points on the potential energy surface, harmonic vibrational frequencies were obtained at their CCSD(T) equilibrium geometries using up to QZ basis sets. All coupled cluster computations were performed via the CFOUR program.^[23]

Density functional theory (DFT) has been commonly utilized in computational quantum chemistry because the correlation effects are included for a low computational cost. However, the reliability of such DFT methods is affected by the quality of the approximate exchange and correlation functionals. Hence, in the present research, we tested the performance of a diverse set of DFT methods (28 popular functionals), using the CCSD(T) results as the calibration. All intrinsic reaction coordinate (IRC) analyses were performed via the MPW1K functional,^[24] which has proved to perform quite well for the $\text{H}_2\text{S} + \text{OH}^{[3]}$ and $\text{H}_2\text{Se} + \text{OH}^{[2]}$ reactions. The DFT computations were performed using the Gaussian16 program.^[25]

3. Results and Discussion

3.1 Structures and Energetics of Stationary Points

The potential energy surface for the $\text{H}_2\text{Te} + \text{OH} \rightarrow \text{TeH} + \text{H}_2\text{O}$ reaction is outlined in Figure 1. The geometries and relative energies for the stationary points on the potential surface will be discussed below. In order to determine the reliability of the single-reference coupled-cluster results, T_1 diagnostic values, proposed by Lee and Taylor,^[26] are evaluated for all the stationary points on the two pathways. Table S1 shows that the T_1 diagnostic values for most structures are modest (less than 0.02). One (**RCB**) is less than 0.04, still fine for an open-shell molecule, as suggested by Taylor.^[26b] As expected the transition states have more challenging electronic structures than the equilibrium geometries.

3.1.1 Reactants (H_2Te and OH)

For the reactants (H_2Te and OH), the bond distances and bond angles obtained with the CCSD(T) method are close to the experimental results. The bond distances for the OH radical are predicted to be 0.980, 0.973, and 0.971 Å with the DZ, TZ, and QZ basis sets, respectively (Figure 2), which converge well toward the experimental result of 0.9697 Å.^[27] The Te-H distances in H_2Te (C_{2v}) are estimated to be 1.668, 1.665, and 1.662 Å, and the H-Te-H bond angles are 90.2°, 90.2°, and 90.4° using the DZ, TZ, and QZ basis sets, respectively (Figure 2). These geometric parameters agree satisfactorily with the experimentally equilibrium structure of H_2Te as follows: $r_e(\text{Te-H}) = 1.651$ Å and $\alpha_e(\text{HTeH}) = 90.3^\circ$.^[28]

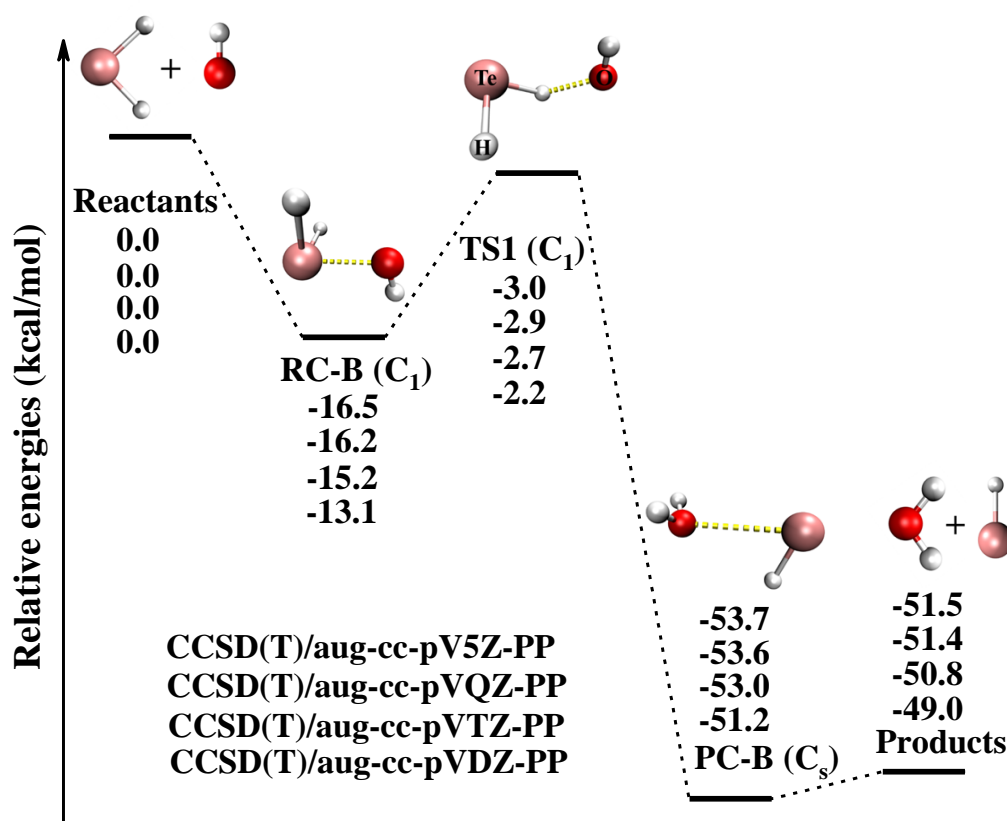


Figure 1. Profile of the CCSD(T) potential energy surface without zero-point vibrational energy (ZPVE) corrections for the $\text{H}_2\text{Te} + \text{OH} \rightarrow \text{H}_2\text{O} + \text{TeH}$ reaction. The 5Z results are single-point energies at the optimized QZ geometries.

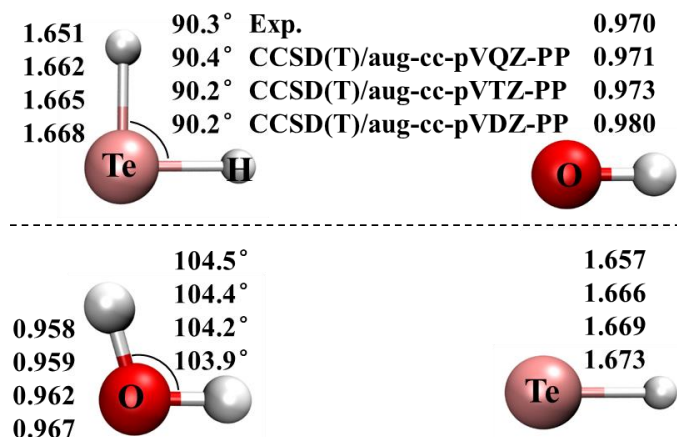


Figure 2. Optimized geometries of the reactants (H_2Te and OH) and products (H_2O and TeH). All bond distances are in Å. The experimental geometries are listed at the top.

3.1.2 Reactant Complex (Entrance Complex)

Analogous to the $\text{H}_2\text{S} + \text{OH}$ and $\text{H}_2\text{Se} + \text{OH}$ reactions,^[2, 3] there are three isomeric reactant complexes (**RC-A**, **RC-B**, and **RC-C**) for the $\text{H}_2\text{Te} + \text{OH} \rightarrow \text{TeH} + \text{H}_2\text{O}$ reaction. Those are illustrated in Figure 3 and Table S2. The isomer **RC-A** ($\text{H}_2\text{Te}\cdots\text{HO}$, in its ${}^2\text{A}'$ electronic state) has a bond between the Te atom and the OH radical (2.889 Å, QZ). The dissociation energy of **RC-A** relative to the reactants (H_2Te and OH) is found to be 2.7 kcal/mol, which is smaller than 3.0, 3.3, and 5.7 kcal/mol for the analogous **RC-A** complexes $\text{H}_2\text{Se}\cdots\text{HO}$, $\text{H}_2\text{S}\cdots\text{HO}$, and $\text{H}_2\text{O}\cdots\text{HO}$, respectively.^[2-4] The isomer **RC-B** is of C_1 symmetry, and a C_s structure (at its ${}^2\text{A}'$ state) lies only 0.1 kcal/mol above. **RC-B** is predicted to have a $\text{H}_2\text{Te}\cdots\text{OH}$ 2c-3e hemi-bond, in which the Te atom and O atom share three electrons. This makes the net $\text{Te}\cdots\text{O}$ bond order 0.5. The $\text{H}_2\text{Te}\cdots\text{OH}$ distance in the **RC-B** isomer is 2.149 Å (QZ), and its energy relative to the reactants (H_2Te and OH) is -16.2 kcal/mol (QZ) or -16.5 kcal/mol (single point energy at 5Z), lower than **RC-A** ($\text{H}_2\text{Te}\cdots\text{HO}$) by 13.8 kcal/mol (Table 1). As a comparison, in the analogous reaction $\text{H}_2\text{Se} + \text{OH}$, **RC-B** ($\text{H}_2\text{Se}\cdots\text{OH}$) is lower than its **RC-A** ($\text{H}_2\text{Se}\cdots\text{HO}$) by only 2.1 kcal/mol.^[2] In reaction $\text{H}_2\text{S} + \text{OH}$, **RC-B** ($\text{H}_2\text{S}\cdots\text{OH}$) is slightly higher than **RC-A** ($\text{H}_2\text{S}\cdots\text{HO}$) by 0.1 kcal/mol.^[3] This may be rationalized in terms of the different electronegativities for Te

(2.1), Se (2.55), and S (2.58).^[29] Since Te has the smallest electronegativity, the $\text{H}_2\text{Te}\cdots\text{HO}$ bonding in **RC-A** is weaker than that in **RC-A** ($\text{H}_2\text{Se}\cdots\text{HO}$) and **RC-A** ($\text{H}_2\text{S}\cdots\text{HO}$), while the $\text{H}_2\text{Te}\cdots\text{OH}$ 2c-3e interaction in **RC-B** is stronger than that in **RC-B** ($\text{H}_2\text{Se}\cdots\text{OH}$) and **RC-B** ($\text{H}_2\text{S}\cdots\text{OH}$).

The third reactant complex isomer, **RC-C** (C_s symmetry at $^2A''$ state), is geometrically different from **RC-C** for $\text{H}_2\text{S} + \text{OH}$ and $\text{H}_2\text{Se} + \text{OH}$. In the S and Se cases, the complexes **RC-C** are formed with hydrogen bond $\text{HSH}\cdots\text{OH}$ and $\text{HSeH}\cdots\text{OH}$.^[2, 3] However, in the present study, because of the small electronegativity of Te, the $\text{HTeH}\cdots\text{OH}$ distance in **RC-C** reaches 3.005 Å, obviously too long to have any significant $\text{H}\cdots\text{O}$ bonding. Instead, structure **RC-C** ($\text{H}_2\text{Te}\cdots\text{OH}$) has a 2c-3e hemi-bond ($\text{Te}\cdots\text{O}$) with the distance of 3.244 Å (QZ) and bond order of 0.5. Irrespective, because of its high energy (above **RC-B** by 14.7 kcal/mol, single point energy at 5Z), the reactant complex **RC-C** for the $\text{H}_2\text{Te} + \text{OH}$ reaction has less chemical significance.

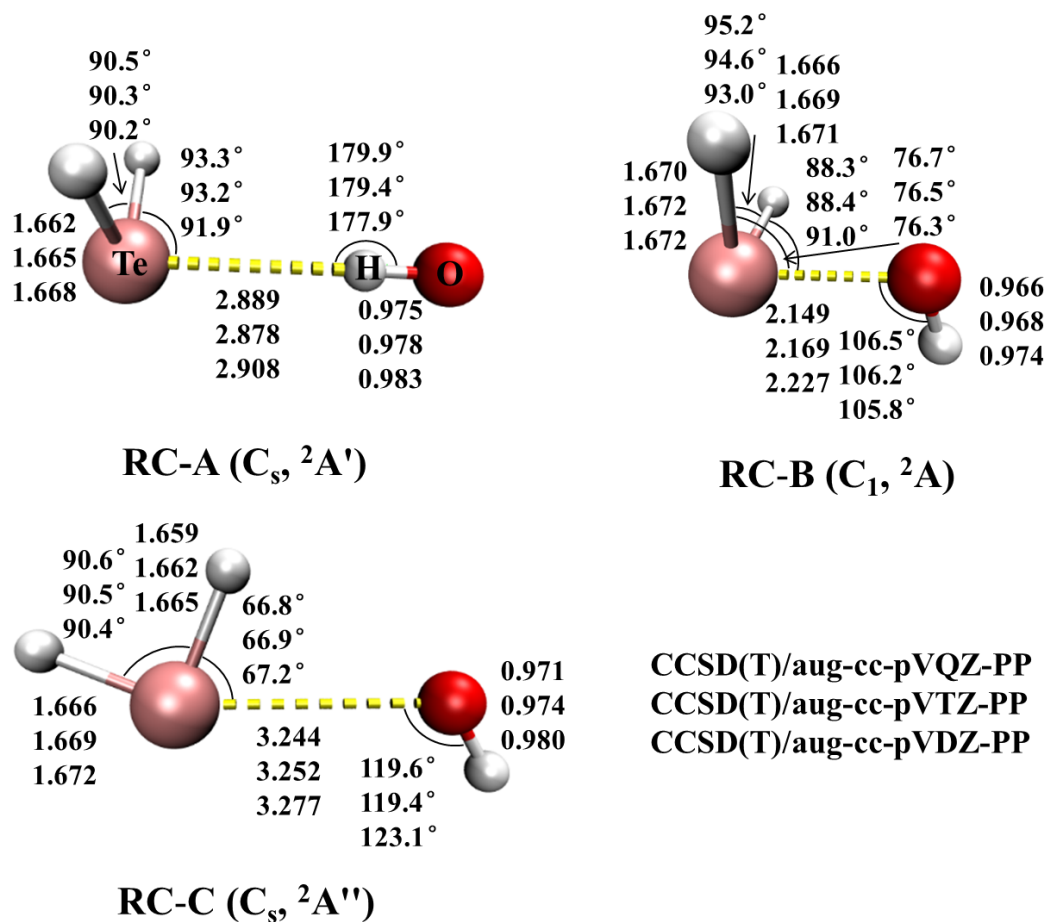


Figure 3. Optimized geometries of the reactant complexes with the CCSD(T) method. All bond distances are in Å.

Table 1. Relative energies (kcal/mol) for the isomers of the reactant complexes and product complexes with the CCSD(T) method and four different basis sets.

Methods	RC-A	RC-B	RC-C	PC-A	PC-B	PC-C
CCSD(T)/aug-cc-pVDZ-PP	10.2	0.0	11.2	1.1	0.6	0.0
CCSD(T)/aug-cc-pVTZ-PP	12.3	0.0	13.3	0.7	0.3	0.0
CCSD(T)/aug-cc-pVQZ-PP	13.5	0.0	14.4	0.7	0.1	0.0
CCSD(T)/aug-cc-pV5Z-PP	13.8	0.0	14.7	0.7	0.1	0.0

3.1.3 Transition State

As shown in Figure 4 and Table S3, an early transition state structure **TS1** for the hydrogen abstraction reaction $\text{H}_2\text{Te} + \text{OH}$ was optimized using the CCSD(T) method. This transition state is geometrically similar to the transition states in the analogous $\text{H}_2\text{Se} + \text{OH}$ and $\text{H}_2\text{S} + \text{OH}$ reactions.^[2,3] With basis sets from DZ to QZ, this **TS1** structure for the title reaction has its hydrogen bond ($\text{HTeH}\cdots\text{OH}$) from 1.771 to 1.720 Å and the $\angle\text{H}\cdots\text{O}-\text{H}$ bond angle from 106.3° to 105.8° . The $\angle\text{Te}-\text{H}\cdots\text{O}$ bond angle is from 104.7° to 99.2° , which is smaller than the corresponding $\angle\text{Se}-\text{H}\cdots\text{O}$ of 128.8° in $\text{H}_2\text{Se} + \text{OH}$,^[2] and the $\angle\text{S}\cdots\text{H}\cdots\text{O}$ angle of 137.5° in $\text{H}_2\text{S} + \text{OH}$.^[3]

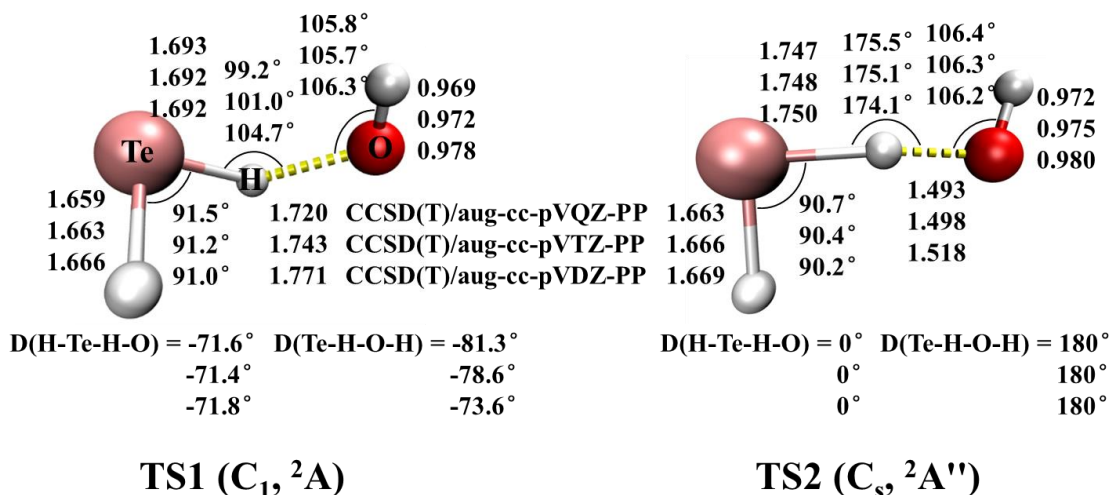


Figure 4. The CCSD(T) optimized geometries of the transition states **TS1** and **TS2** for the $\text{H}_2\text{Te} + \text{OH} \rightarrow \text{H}_2\text{O} + \text{HTe}$ reaction. All bond distances are in Å.

The IRC analysis confirms that structure **TS1** connects the two equilibria **RC-B** (reactant complex) and **PC-B** (product complex). **TS1** lies below the reactants by 2.9 kcal/mol, and the energy span from **RC-B** to **TS1** is 13.3 kcal/mol with the QZ basis sets. With 5Z basis sets, the single point energy of **TS1** is 3.0 kcal/mol below the reactants, and the energy span from **RC-B** is 13.5 kcal/mol.

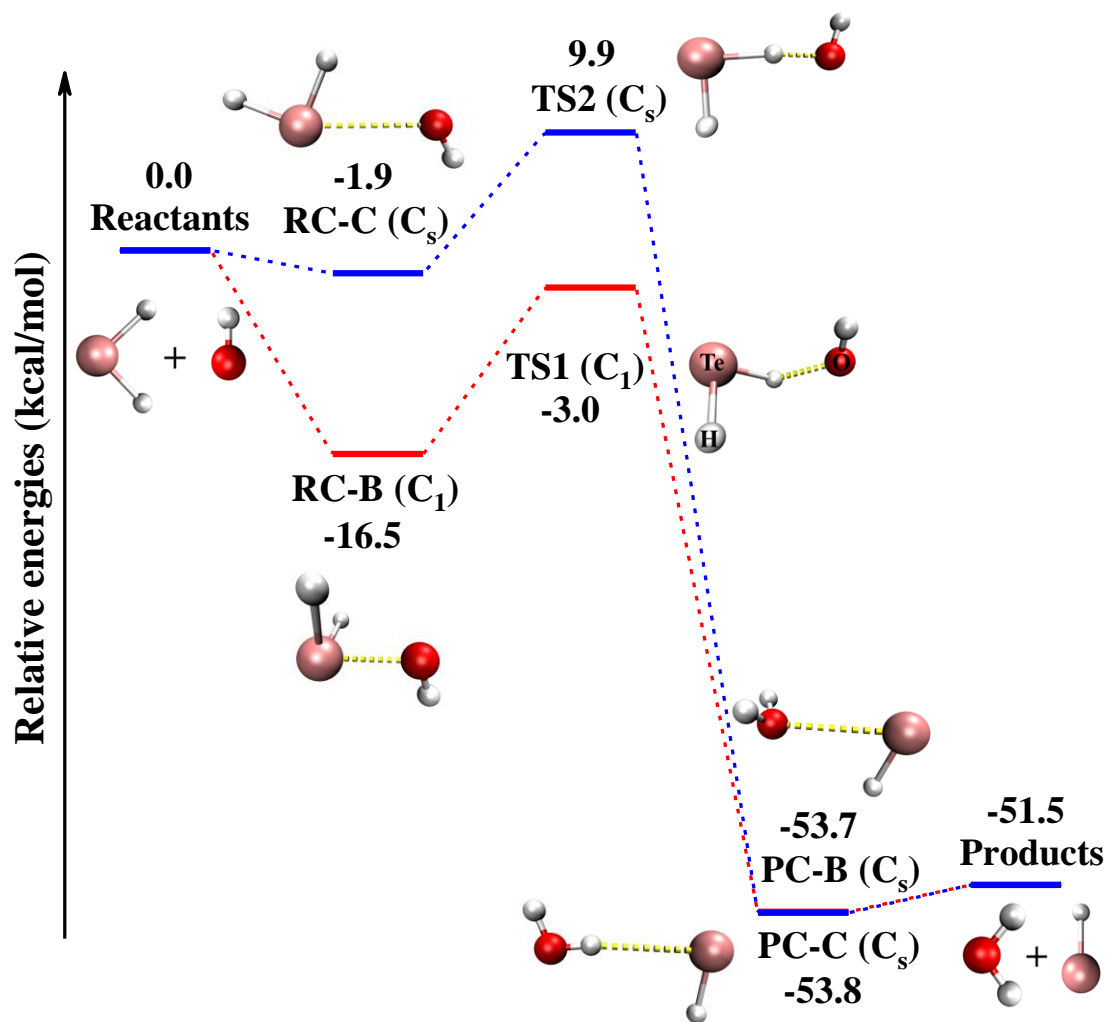


Figure 5. Two possible pathways without ZPVE corrections for the $\text{H}_2\text{Te} + \text{OH}$ reaction. All energies are CCSD(T)/aug-cc-pV5Z-PP single point energies at the QZ optimized geometries.

In addition to the low-lying reaction pathway **Reactants** \rightarrow **RC-B** \rightarrow **TS1** \rightarrow **PC-B** \rightarrow **Products** (red in Figure 5), there exists another higher-lying pathway **Reactants** \rightarrow **RC-C** \rightarrow **TS2** \rightarrow **PC-C** \rightarrow **Products** (blue in Figure 5). This second pathway, confirmed by the IRC analysis, was also found in the analogous reaction $\text{H}_2\text{Se} + \text{OH}$,^[2] but *not* found in $\text{H}_2\text{S} + \text{OH}$.^[3] Similar to that in the $\text{H}_2\text{Se} + \text{OH}$ reaction,^[2] the second transition state **TS2**

is a planar structure with C_s symmetry (Figure 4), a shorter $\text{HTeH}\cdots\text{OH}$ hydrogen bond of 1.493 Å, and a larger $\angle\text{Te-H}\cdots\text{O}$ bond angle of 175.5° than those for **TS1**. Since **TS2** is found to have a significantly higher energy than **TS1** by 12.7 kcal/mol (QZ) or 12.9 kcal/mol (5Z single point energy), the second reaction pathway (blue in Figure 5) is unlikely to be practical.

3.1.4 Product Complex (Exit Complex)

Related to the reactant complexes, there exist three product complexes (**PC-A**, **PC-B**, and **PC-C**) for the $\text{H}_2\text{Te} + \text{OH}$ reaction (Figure 6 and Table S4). These product complex structures are geometrically associated with those for the $\text{H}_2\text{Se} + \text{OH}$ and $\text{H}_2\text{S} + \text{OH}$ reactions.^[2, 3]

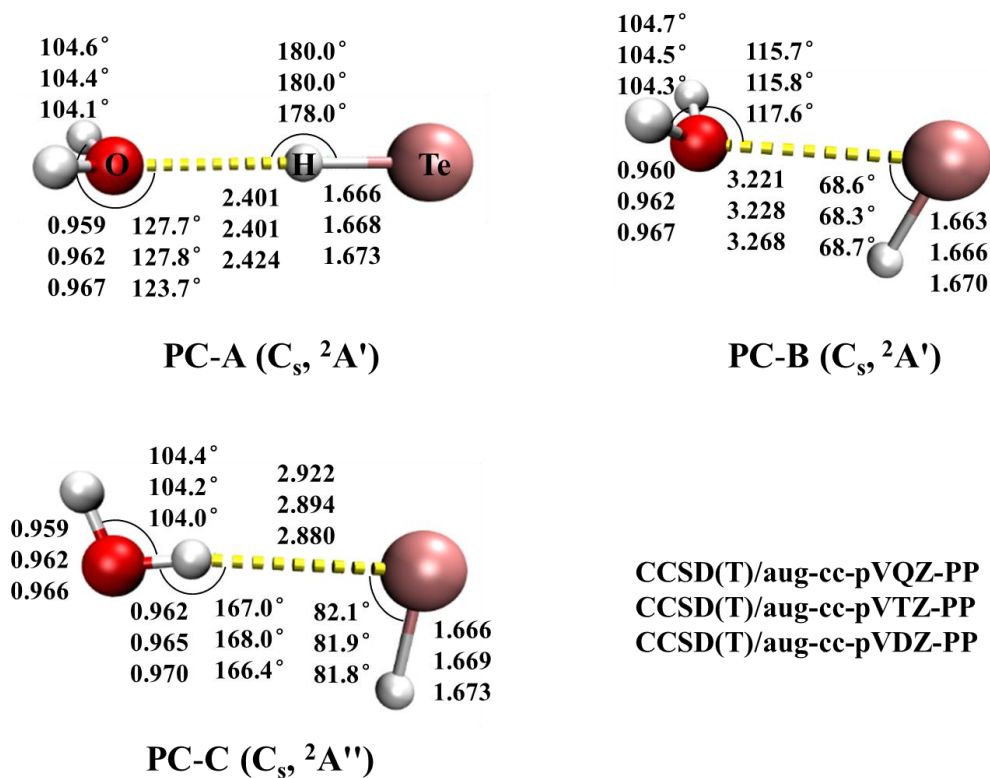


Figure 6. Optimized geometries of the product complexes with the CCSD(T) method. All bond distances are in Å.

As listed in Table 1, the CCSD(T) method predicts that the energy differences among the three product complexes are very small (within 1 kcal/mol), and the **PC-C** structure (HOH \cdots TeH) in its $^2A''$ electronic state is slightly lower than other two. Based on the 5Z single point energies, isomer **PC-A** in its $^2A'$ state with a H₂O \cdots HTe bond lies 0.7 kcal/mol above **PC-C**, while isomer **PC-B** with a hemi-bond H₂O \cdots TeH in its $^2A'$ state lies only 0.1 kcal/mol above **PC-C**. Figure 5 shows that structure **PC-B** connects to the lower transition state **TS1**, while structure **PC-C** connects to the higher-lying transition state **TS2**. Figure 5 also shows that these product complexes lie significantly lower than the reactant complexes. Both isomers **PC-B** and **PC-C** lie below the isolated reactants by more than 53 kcal/mol. The dissociation energies with respect to the isolated products are only 2 kcal/mol, similar to the cases of H₂Se + OH and H₂S + OH.^[2, 3]

3.1.5 Products (TeH and H₂O)

Figure 2 outlines the geometric parameters for the isolated products TeH and H₂O. The experimental results are also listed for comparison. The CCSD(T)/QZ method predicts that the O–H bond length and H–O–H angle in H₂O are 0.959 Å and 104.4°, respectively, very close to the experimental results (0.9578 Å and 104.48°).^[30] The Te–H bond length in TeH free radical is found to be 1.666 Å, in satisfactory agreement with experimental values of $r_e = 1.6567$ Å^[31] or 1.6559 Å.^[32]

From Figure 1, the H₂Te + OH \rightarrow TeH + H₂O reaction is predicted to be exothermic by 49.0, 50.8, 51.4, and 51.5 kcal/mol with the DZ, TZ, QZ, and 5Z basis sets, respectively, suggesting that this reaction is highly thermodynamically favorable, which is expected, since a very weak Te–H bond is exchanged for the very strong O–H bond.

3.2 Vibrational Frequencies and ZPVE Corrections

Table 2 shows the harmonic vibrational frequencies and zero-point vibrational energies (ZPVEs) for the stationary points of the title reaction predicted with the CCSD(T) method with the basis sets from DZ to QZ. The corresponding infrared intensities are

reported in Table S5 (in Supporting Information). For the reactants (H_2Te and OH) and products (H_2O and TeH), our computed CCSD(T) results are consistent with the available experimental vibrational frequencies.^[27, 28, 31-34] Basically, the deviations decrease with the increasing size of the basis sets from DZ to QZ. For water molecule and the radicals TeH and OH , the largest deviation of our QZ results is only 2 cm^{-1} from the experimental harmonic frequencies. For H_2Te , our QZ harmonic frequencies are also in reasonable agreement with the available experimental fundamental frequencies.

Vibrational analyses for the **TS1** structure indicate that there is one and only one imaginary frequency, which is predicted to be $707i$, $802i$, and $866i\text{ cm}^{-1}$ using DZ, TZ, and QZ basis sets, respectively. The IRC analysis shows that **TS1** connects the reactant complex **RC-B** in one direction and the product complex **PC-B** in the other direction.

It can be found from Table 2 that, from DZ to QZ, the ZPVE for the reactants (H_2Te plus OH) range from 12.7 to 12.8 kcal/mol, while the ZPVE for the products (H_2O plus TeH) are in the range from 16.4 to 16.5 kcal/mol. Hence, the ZPVE correction makes the reaction exothermicity decrease by 3.7 (DZ), 3.7 (TZ), and 3.8 (QZ) kcal/mol, and the ZPVE corrected exothermicity decreases to 45.3 (DZ), 47.1 (TZ), and 47.6 (QZ) kcal/mol.

Similarly, the ZPVE corrected relative energies of **RC-B** become -10.1 , -12.0 , and -13.0 kcal/mol with the DZ, TZ, and QZ basis sets, respectively, and the ZPVE corrected relative energies for the product complex (**PC-B**) become -46.7 (DZ), -48.5 (TZ), and -49.0 (QZ) kcal/mol. The ZPVE corrected relative energies for the transition state **TS1** increase to be -0.6 (DZ), -0.9 (TZ), and -1.1 (QZ) kcal/mol. If we apply the QZ ZPVE corrections onto the 5Z single-point energies, the most reliable estimation for the relative energies for **RC-B**, **TS1**, **PC-B**, and products (TeH and H_2O) will become -13.3 , -1.2 , -49.1 , and -47.8 kcal/mol, respectively.

For the high-lying pathway, the imaginary vibrational frequency of **TS2** is reported to be $3096i\text{ cm}^{-1}$ (QZ), much larger in magnitude than that of **TS1** ($866i\text{ cm}^{-1}$, QZ). This could be connected to the corresponding normal modes: the stretching mode for **TS2** and the

rocking mode for **TS1**. As shown in Figure 5, **TS2** connects **RC-C** and **PC-C**. The harmonic vibrational frequencies and ZPVEs for the stationary points (**RC-C**, **TS2**, and **PC-C**) are predicted using QZ basis set, and the **TS2** energy relative to the reactants after the ZPVE correction decreases to 9.6 kcal/mol (QZ).

Table 2. Harmonic vibrational frequencies (cm^{-1}) and ZPVEs (kcal/mol) for the stationary points of the $\text{H}_2\text{Te} + \text{OH}$ reaction from the CCSD(T) method with the aug-cc-pVnZ-PP ($n = \text{D, T, Q}$) basis sets.^a

	ZPVE	ΔZPVE	ΔE	ΔE_{ZPVE}	vibrational frequencies ω								
CCSD(T)/aug-cc-pVDZ-PP													
$\text{H}_2\text{Te} + \text{OH}$	12.7	0.0	0.0	0.0	2141	2132	901	(H_2Te);	3684	(OH)			
RC-B	15.7	3.1	-13.1	-10.1	3722	2115	2084	863	835	601	325	308	156
TS1	14.2	1.6	-2.2	-0.6	3688	2145	1947	889	637	315	268	77	707i
PC-B	17.2	4.5	-51.2	-46.7	3898	3779	2121	1634	184	129	119	69	65
$\text{H}_2\text{O} + \text{TeH}$	16.4	3.7	-49.0	-45.3	3905	3787	1638	(H_2O);	2110	(TeH)			
CCSD(T)/aug-cc-pVTZ-PP													
$\text{H}_2\text{Te} + \text{OH}$	12.7	0.0	0.0	0.0	2145	2137	887	(H_2Te);	3718	(OH)			
RC-B	15.9	3.2	-15.2	-12.0	3754	2112	2068	882	814	624	356	331	190
TS1	14.5	1.7	-2.7	-0.9	3724	2151	1954	872	663	349	292	107	802i
PC-B	17.3	4.6	-53.0	-48.5	3912	3802	2132	1642	201	127	122	73	71
$\text{H}_2\text{O} + \text{TeH}$	16.4	3.7	-50.8	-47.1	3920	3811	1646	(H_2O);	2120	(TeH)			
CCSD(T)/aug-cc-pVQZ-PP													
$\text{H}_2\text{Te} + \text{OH}$	12.8	0.0	0.0	0.0	2153	2146	885	(H_2Te);	3739	(OH)			
RC-B	16.0	3.3	-16.2	-13.0	3772	2118	2070	889	810	633	366	340	199
TS1	14.6	1.8	-2.9	-1.1	3744	2160	1951	870	678	370	308	130	866i
PC-B	17.3	4.6	-53.6	-49.0	3932	3821	2142	1646	202	125	121	72	70
$\text{H}_2\text{O} + \text{TeH}$	16.5	3.8	-51.4	-47.6	3941	3831	1650	(H_2O);	2130	(TeH)			
Experimental results													
					2072	2065	861	$\text{H}_2\text{Te}^{\text{b}}$	3738	OH^{c}			
					3943	3832	1649	$\text{H}_2\text{O}^{\text{d}}$	2128	TeH^{e}			
									2129	TeH^{f}			

^a Relative energies are given with and without ZPVE corrections (in kcal/mol).

^b Fundamental frequencies in Refs. 28 and 33.

^c Harmonic frequencies in Ref. 27.

^d Harmonic frequencies in Ref. 34.

^e Harmonic frequencies in Ref. 32.

^f Harmonic frequencies in Ref. 31.

3.3 Potential energy surface with spin-orbit coupling correction

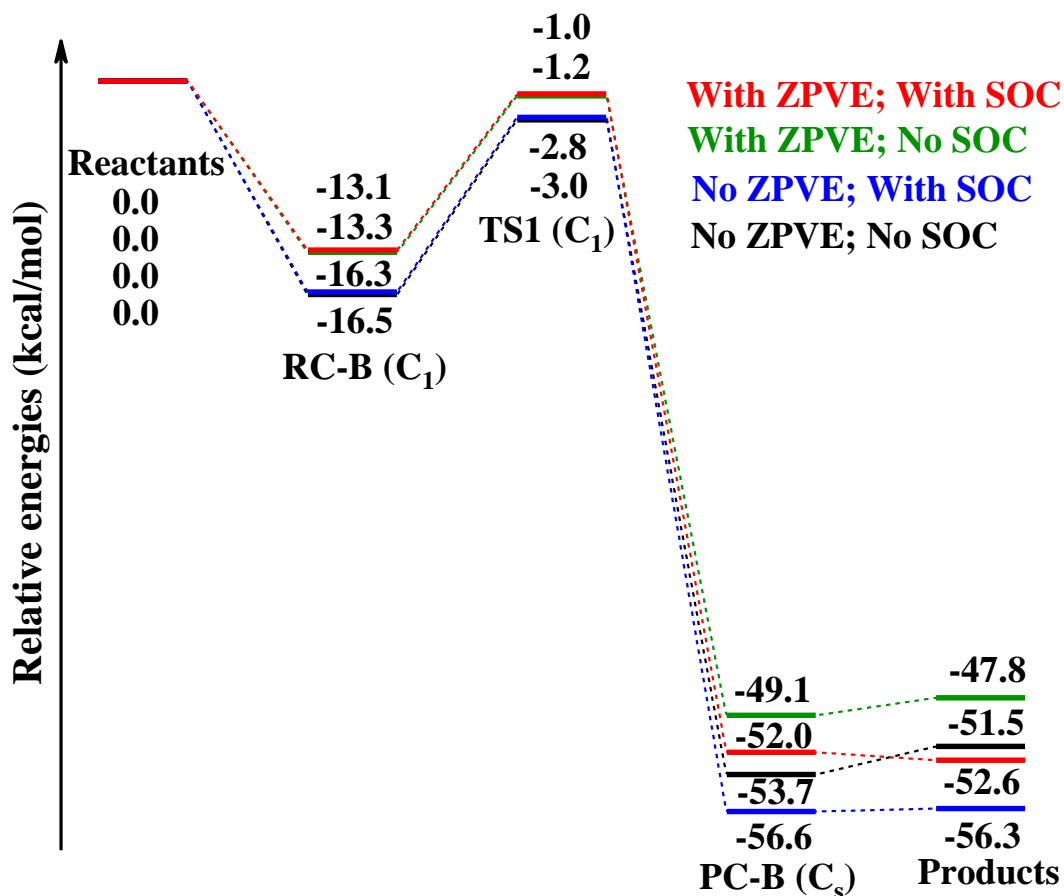


Figure 7. Five stationary points on the potential energy surface for the $\text{H}_2\text{Te} + \text{OH}$ reaction. The single-point energies with 5Z at the optimized QZ geometries are corrected by ZPVE and spin-orbit coupling (SOC) effects.

For systems involving the heavy element tellurium, spin-orbit coupling (SOC) effects are noteworthy for the predicted energetics. In this research, we adopt the Breit-Pauli operator to provide SOC corrections,^[35] using the MOLPRO program package.^[36] The full valence complete active space self-consistent field (CASSCF) wave functions are used for this purpose, in which aug-cc-pVQZ-PP basis sets were employed. On the low-lying reaction pathway, spin-orbit coupling correction only slightly affects the relative energy of transition state **TS1** and entrance complex **RC-B**. However, this correction has noticeable effect on the reaction energy and the **PC-B** relative energy. Our

theoretical SOC corrections for the reactants (mainly the OH radical), **RC-B**, **TS1**, **PC-B**, and the product (the TeH radical) are predicted to be 68.3, 0.4, 1.7, 1082.2, and 1747.3 cm^{-1} (*i.e.* 0.2, 0.0, 0.0, 3.1, and 5.0 kcal/mol), respectively. After spin-orbit coupling correction, the relative energies of **RC-B**, **TS1**, **PC-B**, and the products become -16.3, -2.8, -56.6, and -56.3 kcal/mol, respectively, shown in Figure 7 as blue entries. With both ZPVE and spin-orbit coupling corrections, the relative energies of **RC-B**, **TS1**, **PC-B**, and the products are -13.1, -1.0, -52.0, and -52.6 kcal/mol, respectively.

3.4 Performance of DFT Methods

DFT methods have been widely utilized in computational chemistry. However, various DFT functionals may yield quite different results because they are constructed with different strategies. A general study of DFT abilities in prediction of molecular structures and reaction barrier heights has been reported by Truhlar et al.^[37] We also compared the performance of a series of DFT functionals in our previous studies on the $\text{H}_2\text{O} + \text{OH}$, $\text{H}_2\text{S} + \text{OH}$, and $\text{H}_2\text{Se} + \text{OH}$ hydrogen abstraction reactions,^[2-4] and we will do so for the Te system in the present paper using 28 popular DFT functionals^[24,38-69] along with the TZ basis set. The ZPVE corrected DFT relative energies of all stationary points in the favorable pathway are depicted in Table 3. The "gold standard" CCSD(T)/5Z method are also provided at the bottom as a calibration. (The DFT energies without the ZPVE corrections are listed in Table S6).

In Table 3, most DFT functionals predict the reaction energy in a range from -45 to -48 kcal/mol, in agreement with the CCSD(T) result of -47.8 kcal/mol. There are only a few exceptions, including TPSSh, M06-L, and BH&HLYP (predicting it < 43 kcal/mol) and M06-2X (predicting it > 55 kcal/mol). Similarly, most of the DFT functionals predict the energy of product complex **PC-B** close to the CCSD(T) result (-49.1 kcal/mol), except for TPSSh and BH&HLYP (predicting it < 44 kcal/mol) and M06-2X (predicting it > 57 kcal/mol).

Table 3. Relative energies (kcal/mol) with *ZPVE correction* for the stationary points on the potential energy surface predicted by 28 DFT functionals with the aug-cc-pVTZ-PP basis sets. The CCSD(T)/5Z results are listed for comparison. The DFT functionals are arranged in order of the energy of **TS1**.

Methods	H ₂ Te+OH	RC-B	TS1	TS1 vs RC-B	PC-B	H ₂ O+HTe	HF%	Ref
BH&HLYP	0.0	-4.0	0.1	4.2	-43.5	-42.9	50	38
MPW1K	0.0	-7.5	-0.5	6.9	-44.6	-44.1	42.8	24
MPWK CIS1K	0.0	-8.4	-0.7	7.6	-46.7	-46.2	41	39
BB1K	0.0	-9.4	-0.9	8.4	-45.8	-45.4	42	40
MPWB1K	0.0	-9.9	-1.4	8.4	-46.4	-45.4	44	41
M05-2X	0.0	-11.5	-2.3	9.2	-54.2	-52.3	56	42
M06-2X	0.0	-13.1	-2.4	10.7	-57.1	-54.6	54	43
BMK	0.0	-12.8	-2.6	10.3	-48.2	-47.8	42	44
ω B97-X	0.0	-12.3	-2.7	9.6	-48.2	-45.7	LC ^a	45
ω B97	0.0	-12.1	-2.9	9.2	-48.0	-45.2	LC ^a	45
CAM-B3LYP	0.0	-12.2	-3.0	9.2	-47.7	-46.8	19-65	46
ω B97-XD	0.0	-12.2	-3.1	9.2	-47.5	-45.9	LC ^a	47
mPW1PW91	0.0	-15.3	-4.1	11.2	-46.0	-45.4	25	48,49
M05	0.0	-16.9	-5.0	11.9	-47.9	-46.1	28	50
PBE0	0.0	-16.5	-5.2	11.3	-46.8	-45.8	25	51-53
B3PW91	0.0	-16.3	-5.2	11.1	-46.1	-46.0	20	49,54
B3LYP	0.0	-16.0	-5.5	10.5	-46.3	-45.8	20	54
HSEh1PBE	0.0	-16.4	-5.5	11.0	-46.2	-45.0	25	55-61
B98	0.0	-16.8	-5.9	10.9	-47.7	-46.4	21.98	62
MPW3LYP	0.0	-16.7	-6.1	10.6	-47.0	-45.8	21.8	41,48
TPSSh	0.0	-17.8	-6.6	11.3	-42.7	-41.8	10	63
M06	0.0	-17.7	-6.6	11.1	-48.4	-45.9	27	43
TPSS1KCIS	0.0	-17.8	-6.6	11.2	-44.6	-43.9	13	64
MPW1KCIS	0.0	-19.1	-8.6	10.5	-48.6	-48.1	15	39
M06-L	0.0	-19.9	-8.8	11.1	-44.3	-42.3	0	65
VSXC	0.0	-19.6	-11.4	8.2	-50.4	-46.1	0	66
BLYP	0.0	-22.1	-12.3	9.7	-47.0	-46.5	0	67,68
BP86	0.0	-24.2	-14.0	10.2	-48.3	-47.3	0	68,69
CCSD(T)/5Z	0.0	-13.3	-1.2	12.1	-49.1	-47.8	-	-

^a For the LC methods, the percentage of H-F component varies with the long-range corrections.

Unlike products and **PC-B**, for the transition state **TS1**, only six functionals (MPWB1K, BB1K, MPWKIS1K, MPW1K, M05-2X, and M06-2X) predict the relative energy in agreement with the CCSD(T)/5Z value (-1.2 kcal/mol) to within ~ 1 kcal/mol, and the other functionals predict it in a wide range (from 0.1 to -14.0 kcal/mol). The performance of the functionals seems to correlate roughly with the percentage of Hartree-Fock (HF) exchange term. For example, all the functionals with less than 28% HF component predicts the **TS1** relative energy lower than -4.1 kcal/mol, among which the BP86 functional (with 0% HF component) predicts the smallest value (-14.0 kcal/mol). This was also true for the $\text{H}_2\text{Se} + \text{OH}$ and $\text{H}_2\text{S} + \text{OH}$ reactions.^[2, 3] Similar to **TS1**, the relative energy of the reactant complex **RC-B** predicted by these 28 functionals is in a broad range (from -4.0 to -24.2 kcal/mol). Only eight functionals (lines 6–13 in Table 3) predict it close to the CCSD(T)/5Z result (-13.3 kcal/mol), i.e., within 2 kcal/mol.

Interestingly, most DFT methods predict the molecular geometries, including **TS1** and **RC-B**, comparable with the CCSD(T) results. The predicted geometries by 28 DFT functionals for **TS1** are compared with the CCSD(T) geometry (Table S7). For H–Te and O–H bond lengths, there only exist small deviations (< 0.01 Å) via most DFT functionals. For the weak interaction $\text{Te}\cdots\text{H}$, the distance deviations are generally within 0.02 Å, while the deviations for the $\text{H}\cdots\text{O}$ distance appear somewhat larger, but most of them still within 0.06 Å. The other stationary points for the title reaction display to same pattern. For example, Figure S4 shows the geometries of the reactant complexes and the product complexes predicted by M06-2X and MPWB1K, and these geometries are close to the CCSD(T)/QZ result (Figure 3 and Figure 6). Based on the small deviations of DFT geometries, it is anticipated that the single point energy strategy is applicable to predict the reasonable energetics. Indeed, Table S8 shows that the relative energy of **TS1** at the CCSD(T)/QZ//DFT/TZ level is in a narrow range (-2.3 to -3.2 kcal/mol). For example, the BLYP relative energy of **TS1** at the BLYP geometry is -14.2 kcal/mol (Table S6),

while the CCSD(T)/QZ single-point energy at the BLYP/TZ geometry becomes -2.8 kcal/mol (Table S8), much closer to the CCSD(T) result (-3.0 kcal/mol).

3.5 Comparisons with $\text{H}_2\text{Se} + \text{OH}$, $\text{H}_2\text{S} + \text{OH}$ and $\text{H}_2\text{O} + \text{OH}$

For the title reaction $\text{OH} + \text{H}_2\text{Te} \rightarrow \text{H}_2\text{O} + \text{HTe}$, a hydrogen atom is abstracted from hydrogen telluride to the OH radical, analogous to our previously studied hydrogen abstraction reactions $\text{OH} + \text{H}_2\text{Se}$, $\text{OH} + \text{H}_2\text{S}$, and $\text{OH} + \text{H}_2\text{O}$.^[2-4] In Figure 8 the favorable pathways of these four analogous reactions at the CCSD(T)/5Z level are compared.

As expected, for the symmetrical $\text{OH} + \text{H}_2\text{O} \rightarrow \text{H}_2\text{O} + \text{OH}$ reaction, the reaction energy is absolutely zero. The other analogous reactions are all exothermic, and the energy released increase from the $\text{OH} + \text{H}_2\text{S}$ reaction (27.1 kcal/mol), to the $\text{OH} + \text{H}_2\text{Se}$ reaction (37.7 kcal/mol), and to the $\text{OH} + \text{H}_2\text{Te}$ reaction (47.8 kcal/mol). This is roughly equal to the difference between the bond dissociation energy (BDE) for the H–OH bond (117.6 kcal/mol)^[70] and BDEs for the H–XH (X = S, Se, Te) bonds, which are 89.9 kcal/mol for H–SH,^[71] 79.0 kcal/mol for H–SeH,^[72] and 65.0 kcal/mol for H–TeH.^[73]

Both the reactant complex and product complex for the $\text{H}_2\text{Te} + \text{OH}$ reaction have more in common with those for the $\text{H}_2\text{Se} + \text{OH}$ reaction than with those for $\text{H}_2\text{S} + \text{OH}$ and $\text{H}_2\text{O} + \text{OH}$. For the $\text{H}_2\text{O} + \text{OH}$ and $\text{H}_2\text{S} + \text{OH}$ reactions, the low-lying complexes are formed with hydrogen-bond,^[3, 4] while the complexes at the lower-lying pathway for the $\text{H}_2\text{Se} + \text{OH}$ and $\text{H}_2\text{Te} + \text{OH}$ reaction are formed with the 2c-3e hemibond.^[2] This is explained since the O and S atoms are more electronegative than the Se and Te atoms. Thus, we can see in Figure 8 that the relative energy of reactant complex $\text{H}_2\text{O}\cdots\text{HO}$ is lower than that of reactant complex $\text{H}_2\text{S}\cdots\text{HO}$, since the former has stronger hydrogen bond. However, we cannot directly compare the strength of the 2c-3e hemibond with that of the hydrogen bond, and it is not surprising that the energy order of the reactant complexes in Figure 8 is not entirely consistent with the order of chalcogen elements in periodic table.

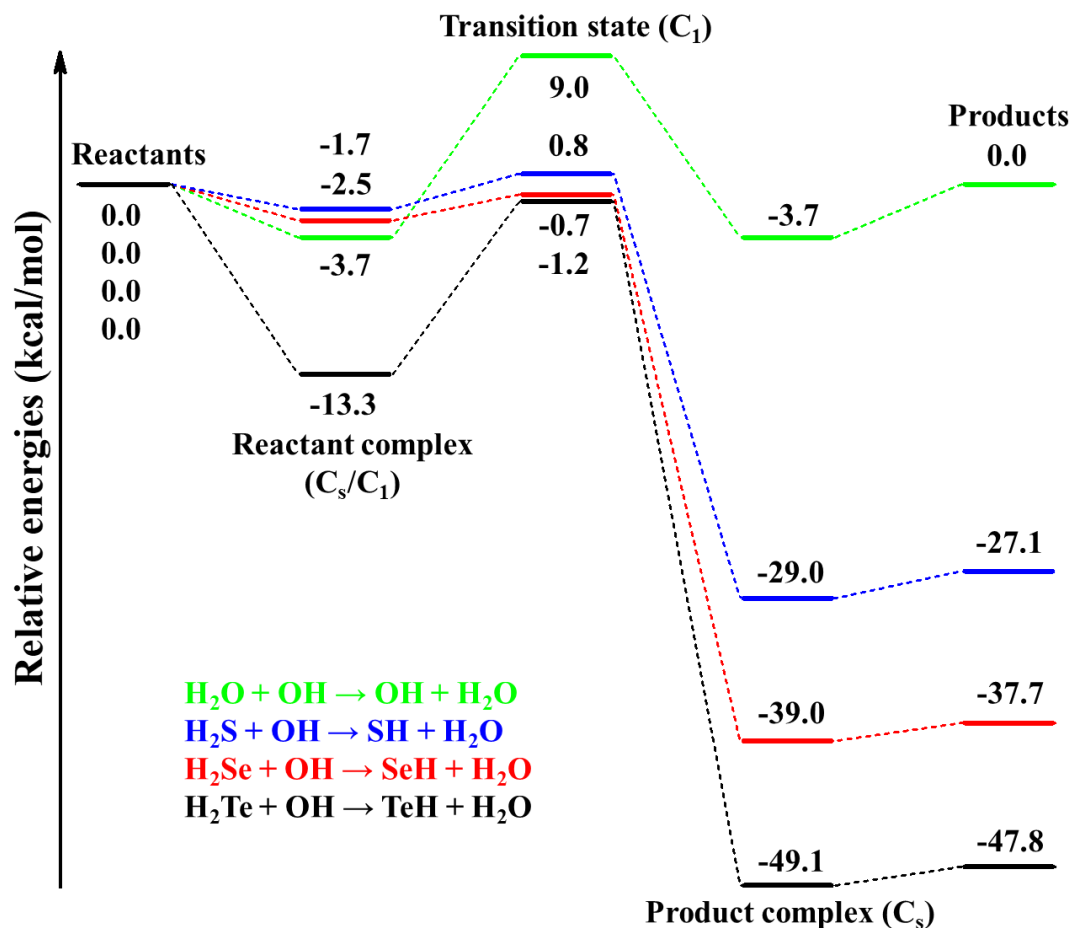


Figure 8. Comparison of the potential energy surface of the H₂Te + OH reaction with the H₂Se + OH,^[2] H₂S + OH,^[3] and H₂O + OH^[4] reactions at the CCSD(T)/5Z level (with ZPVE corrections).

As shown in Figure 8, the energy of the transition state **TS1** for the H₂Te + OH reaction is below the reactants H₂Te + OH by 1.2 kcal/mol. Similarly, the transition state for the H₂Se + OH reaction is also below its reactants H₂Se + OH, but by a smaller value 0.7 kcal/mol.^[2] On the contrary, the transition states for the H₂S + OH and H₂O + OH reactions are higher than their reactants, by 0.8 and 9.0 kcal/mol, respectively.^[3, 4] The **TS1** energies in the order of H₂O > H₂S > H₂Se > H₂Te are also observed by Kumar and Francisco in the CH₂OO + H₂X (X = O, S, Se, Te) reaction.^[15] They ascribed this energy order to the increasing X–H bond length or atomic radius, and thus the decreasing X–H

bond strength as moving down the chalcogen group. This implies that H₂Te would react faster with the OH radical than its chalcogen congeners.

4. Conclusions

We have examined the structures, energetics, and vibrational frequencies for the stationary points on the potential surface of the hydrogen abstraction reaction H₂Te + OH using the "gold standard" CCSD(T) method with basis sets up to aug-cc-pV5Z-PP. With the ZPVE corrections, this reaction is found to be exothermic by 47.8 kcal/mol.

The low-lying transition state **TS1** for the H₂Te + OH reaction lies below the reactants by 1.2 kcal/mol. Thus it is a submerged transition state. For comparison, the transition states for the analogous H₂X + OH (X = Se, S, O) reactions lie -0.7 (H₂Se), +0.8 (H₂S), and +9.0 (H₂O) kcal/mol with respect to the appropriate reactants, and these relative energies are correlated with the corresponding X-H (X = O, S, Se, and Te) bond distances.^[15] Like the H₂Se + OH reaction, there is another pathway for the H₂Te + OH reaction, but its transition state **TS2** has a significantly high energy (+9.8 kcal/mol) relative to the reactants.

With different bonding scheme, we found three reactant complexes and three product complexes for the H₂Te + OH reaction, and this is often similar to the cases of the H₂S + OH and H₂Se + OH reactions. However, for H₂Te + OH and H₂Se + OH, the lowest-energy reactant complex **RC-B** is a 2c-3e hemibonded structure, whereas for H₂S + OH and H₂O + OH, the lowest corresponds to a conventional hydrogen-bonded structure. For the product complex, although the most favored structure for the H₂Te + OH reaction is **PC-C** with a HOH...TeH bond, the hemi-bonded structure H₂O...TeH (**PC-B**) has nearly degenerate energy to **PC-C** (< 0.1 kcal/mol with 5Z), and the product complex isomers for H₂S + OH and H₂Se + OH have a similar energy order. Thus, the observation of the energy-favorable complexes **RC-B** (H₂Te...OH) or **PC-C** (HTe...HOH) with matrix isolation spectroscopy would be most welcome.

The consideration of spin-orbit coupling effect changes the relative energies by 3 ~ 5 kcal/mol for the products (TeH plus H₂O) and **PC-B**, but not much for **RC-B** and **TS1**. With ZPVE and spin-orbit coupling corrections, the energies of **RC-B**, **TS1**, **PC-B**, and products relative to the reactants are estimated to be -13.1, -1.0, -52.0, and -52.6 kcal/mol, respectively.

The systematic tests for 28 DFT methods indicate that different functionals predict quite different transition state energies from 0.1 to -14.0 kcal/mol, which correlates with the HF component in the exchange term. It seems that MPWB1K and M06-2X predict the **TS1** energy close to the CCSD(T) result. The strategy of using the CCSD(T) single point energy at the DFT optimized geometry would predict a reasonable reaction energy barrier in this case.

Supporting Information

Profile of the CCSD(T) potential energy surface without ZPVE corrections for the H₂Te + OH reaction (in kJ/mol) (Figure S1); Two possible pathways without ZPVE corrections (in kJ/mol) (Figure S2); Five stationary points on the potential energy surface corrected by ZPVE and SOC effects (in kJ/mol) (Figure S3); Optimized geometries of the reactant and product complexes with DFT (M06-2X and MPWB1K) functionals (Figure S4); Comparison of the potential energy surface of the H₂Te + OH reaction with the H₂Se + OH, H₂S + OH, and H₂O + OH reactions with ZPVE corrections (in kJ/mol) (Figure S5); Comparison of the potential energy surface of the H₂Te + OH reaction with three analogous reactions without ZPVE corrections (Figure S6); T1 diagnostic values of all the stationary points for the two pathways (Table S1); CCSD(T) optimized geometries of the reactant complex (Table S2); CCSD(T) optimized geometries of the transition states **TS1** and **TS2** (Table S3); CCSD(T) optimized geometries of the product complex (Table S4); Harmonic vibrational frequencies and infrared intensities for the stationary points (Table S5); Relative energies for the stationary points predicted by 28 DFT functionals without

ZPVE corrections (Table S6); Predicted geometries for **TS1** by 28 DFT functionals (Table S7); Barrier heights using the CCSD(T)/aug-cc-pVQZ-PP single-point energies at the geometries predicted by 28 DFT functionals (Table S8).

Acknowledgments

This work was supported by the Natural Science Foundation of Sichuan Province (2022NSFSC1826; 2022NSFSC1243) and the Guangdong Basic and Applied Basic Research Foundation (2021A1515010382). The research at the University of Georgia was supported by the US Department of Energy, Basic Energy Sciences Division of Chemistry, Computational and Theoretical Chemistry (CTC) Program, Contract No. DE-SC0018412.

References

- (1) Isaksen, I. S. A.; Dalsøren, S. B. Atmospheric Science. Getting A Better Estimate of An Atmospheric Radical. *Science* **2011**, *331*, 38–39.
- (2) Tang, M.; Chen, X.; Xie, Y.; Schaefer, H. F. The Hydrogen Abstraction Reaction $\text{H}_2\text{Se} + \text{OH} \rightarrow \text{H}_2\text{O} + \text{SeH}$: Comparison with the Analogous Hydrogen Sulfide and Water Reactions. *Inorg. Chem.* **2019**, *58*, 2069–2079.
- (3) Tang, M.; Chen, X.; Sun, Z.; Xie, Y.; Schaefer, H. F. The Hydrogen Abstraction Reaction $\text{H}_2\text{S} + \text{OH} \rightarrow \text{H}_2\text{O} + \text{SH}$: Convergent Quantum Mechanical Prediction. *J. Phys. Chem. A* **2017**, *121*, 9136–9145.
- (4) Gao, A.; Li, G.; Peng, B.; Xie, Y.; Schaefer, H. F. The Symmetric Exchange Reaction $\text{OH} + \text{H}_2\text{O} \rightarrow \text{H}_2\text{O} + \text{OH}$: Convergent Quantum Mechanical Prediction. *J. Phys. Chem. A* **2016**, *120*, 10223–10230.
- (5) Goryacheva, O. A.; Novikova, A. S.; Drozd, D. D.; Pidenko, P. S.; Ponomaryeva, T. S.; Bakal, A. A.; Mishra, P. K.; Beloglazova, N. V.; Goryacheva, I. Y. Water-dispersed Luminescent Quantum Dots for miRNA Detection. *Trend. Anal. Chem.* **2019**, *111*, 197–205.

- (6) Ba, L. A.; Döring, M.; Jamier, V.; Jacob, C. Tellurium: An Element with Great Biological Potency and Potential. *Org. Biomol. Chem.* **2010**, *8*, 4203–4216.
- (7) Shen, M.; Jia, W.; You, Y.; Hu, Y.; Li, F.; Tian, S.; Li, J.; Jin, Y.; Han, D. Luminescent Properties of CdTe Quantum Dots Synthesized using 3-mercaptopropionic Acid Reduction of Tellurium Dioxide Directly. *Nanoscale Res. Lett.* **2013**, *8*, 253–258.
- (8) Stürzenbaum, S. R.; Höckner, M.; Panneerselvam, A.; Levitt, J.; Bouillard, J. S.; Taniguchi, S.; Dailey, L. A.; Khanbeigi, R. A.; Rosca, E. V.; Thanou, M.; Suhling, K.; Zayats, A. V.; Green, M. Biosynthesis of Luminescent Quantum Dots in An Earthworm. *Nat. Nanotechnol.* **2013**, *8*, 57–60.
- (9) Feng, L.; Kuang, H.; Yuan, X.; Huang, H.; Yi, S.; Wang, T.; Deng, K.; Tang, C.; Zeng, Y. A Novel Method for Aqueous Synthesis of CdTe Quantum Dots. *Spectrochim Acta A* **2014**, *123*, 298–302.
- (10) Kumar, B. J.; Kumar, D. S.; Mahesh, H. M. A Facile Single Injection Hydrothermal Method for the Synthesis of Thiol Capped CdTe Quantum Dots as Light Harvesters. *J. Lumin.* **2016**, *178*, 362–367.
- (11) Fard-Fini, S. A.; Salavati-Niasari, M.; Mohandes, F. Sonochemical and Hydrothermal Synthesis of PbTe Nanostructures with the Aid of A Novel Capping Agent. *Mater. Res. Bull.* **2013**, *48*, 4332–4338.
- (12) Yang, S.; Cho, K.; Yun, J.; Choi, J.; Kim, S. Thermoelectric Characteristics of γ -Ag₂Te Nanoparticle Thin Films on Flexible Substrates. *Thin Solid Films* **2017**, *641*, 65–68.
- (13) Petragnani, N.; Lo, W.-L. Tellurium in Organic Synthesis. *Phosphorus Sulfur* **1998**, *136*, 91–106.
- (14) Franke, S. M.; Rosenzweig, M. W.; Heinemann, F. W.; Meyer, K. Reactivity of Uranium(III) with H₂E (E = S, Se, Te): Synthesis of A Series of Mononuclear and Dinuclear Uranium(IV) Hydrochalcogenido Complexes. *Chem. Sci.* **2015**, *6*, 275–282.
- (15) Kumar, M.; Francisco, J. S. Heteroatom Tuning of Bimolecular Criegee Reactions

and Its Implications. *Angew. Chem. Int. Ed.* **2016**, *55*, 13432–13435.

(16) Salih, E.; Ayesh, A. I. First Principle Investigation of H₂Se, H₂Te and PH₃ Sensing Based on Graphene Oxide. *Phys. Lett. A* **2020**, *384*, 126775.

(17) Purvis, G. D.; Bartlett, R. J. A Full Coupled-Cluster Singles and Doubles Model: the Inclusion of Disconnected Triples. *J. Chem. Phys.* **1982**, *76*, 1910–1918.

(18) Scuseria, G. E.; Janssen, C. L.; Schaefer, H. F. An Efficient Reformulation of the Closed-Shell Coupled Cluster Single and Double Excitation (CCSD) Equations. *J. Chem. Phys.* **1988**, *89*, 7382–7387.

(19) Raghavachari, K.; Trucks, G. W.; Pople, J. A.; Head-Gordon, M. Fifth-Order Perturbation Comparison of Electron Correlation Theories. *Chem. Phys. Lett.* **1989**, *157*, 479–483.

(20) Dunning, T. H. Gaussian Basis Sets for Use in Correlated Molecular Calculations I: the Atoms Boron through Neon and Hydrogen. *J. Chem. Phys.* **1989**, *90*, 1007–1023.

(21) Kendall, R. A.; Dunning, T. H.; Harrison, R. J. Electron Affinities of the First-Row Atoms Revisited. Systematic Basis Sets and Wave Functions. *J. Chem. Phys.* **1992**, *96*, 6796–6806.

(22) Peterson, K. A.; Figgen, D.; Goll, E.; Stoll, H.; Dolg, M. Systematically Convergent Basis Sets with Relativistic Pseudopotentials. II. Small-Core Pseudopotentials and Correlation Consistent Basis Sets for the post-*d* Group 16–18 Elements. *J. Chem. Phys.* **2003**, *119*, 11113–11123.

(23) Stanton, J. F.; Gauss, J.; Harding, M. E.; Szalay, P. G. *CFOUR, A Quantum Chemical Program Package*, **2010**. For the current version see <http://www.cfour.de>.

(24) Lynch, B. J.; Fast, P. L.; Harris, M.; Truhlar, D. G. Adiabatic Connection for Kinetics. *J. Phys. Chem. A* **2000**, *104*, 4811–4815.

(25) Frisch, M. J.; Trucks, G. W.; Schlegel, H. B.; Scuseria, G. E.; Robb, M. A.; Cheeseman, J. R.; Scalmani, G.; Barone, V.; Petersson, G. A. et al. *Gaussian 16*, Revision C.01; Gaussian, Inc., Wallingford CT, **2019**.

- (26) (a) Lee, T. J.; Taylor, P. R. A Diagnostic for Determining the Quality of Single-Reference Electron Correlation Methods. *Int. J. of Quantum Chem.* **1989**, *23*, 199–207; (b) Taylor, P. R. *Private communication*.
- (27) Huber, K. P.; Herzberg, G. *Molecular Spectra and Molecular Structure: IV. Constants of Diatomic Molecules*; Van Nostrand Reinhold: New York, 1979.
- (28) Flaud, J. M.; Arcas, Ph.; Bürger, H.; Polanz, O.; Halonen, L. High Resolution Study of the ν_2 , $2\nu_1$, $\nu_1 + \nu_3$, and $2\nu_3$ Bands of Hydrogen Telluride: Determination of Equilibrium Rotational Constants and Structure. *J. Mol. Spectrosc.* **1997**, *183*, 310–335.
- (29) *CRC Handbook of Chemistry and Physics, Internet Version 2005*, David R. Lide, ed., <<http://www.hbcernetbase.com>>, CRC Press, Boca Raton, FL, 2005.
- (30) Hoy, A. R.; Bunker, P. R. A Precise Solution of the Rotation Bending Schrödinger Equation for a Triatomic Molecule with Application to the Water Molecule. *J. Mol. Spectrosc.* **1979**, *74*, 1–8.
- (31) Yu, S.; Shayesteh, A.; Fu, D.; Bernath, P. F. Infrared and Near Infrared Emission Spectra of TeH and TeD. *J. Mol. Spectrosc.* **2005**, *230*, 105–116.
- (32) Gillett, D. A.; Towle, J. P.; Islam, M.; Brown, J. M. The Infrared Spectrum of Isotopomers of the TeH Radical, Observed by CO Laser Magnetic Resonance. *J. Mol. Spectrosc.* **1994**, *163*, 459–482.
- (33) Flaud, J.-M.; Betrencourt, M.; Arcas, Ph.; Bürger, H.; Polanz, O.; Lafferty, W. J. Simultaneous Analysis of the $2\nu_2$, ν_1 , and ν_3 Bands of Hydrogen Telluride. *J. Mol. Spectrosc.* **1997**, *182*, 396–420.
- (34) Plíva, J.; Špirko, V.; Papoušek, D. Anharmonic Potential Functions of Polyatomic Molecules. Part VII. Iterational Calculation of Anharmonic Corrections to Fundamental Frequencies. *J. Mol. Spectry.* **1967**, *23*, 331–342.
- (35) Berning, A.; Schweizer, M.; Werner, H.-J.; Knowles, P. J.; Palmieri, P. Spin-orbit Matrix Elements for Internally Contracted Multireference Configuration Interaction Wavefunctions. *Mol. Phys.* **2000**, *98*, 1823–1833.

- (36) Werner, H.-J.; Knowles, P. J.; Knizia, G.; Manby, F. R.; Schütz, M. et al., MOLPRO, version **2010.1**, a package of ab initio programs, see <http://www.molpro.net>.
- (37) Zheng, J.; Zhao, Y.; Truhlar, D. G. The DBH24/08 Database and Its Use to Assess Electronic Structure Model Chemistries for Chemical Reaction Barrier Heights. *J. Chem. Theory Comput.* **2009**, *5*, 808–821.
- (38) Beck, A. D. A New Mixing of Hartree-Fock and Local Density-Functional Theories. *J. Chem. Phys.* **1993**, *98*, 1372–1377.
- (39) Zhao, Y.; González-García, N.; Truhlar, D. G. Benchmark Database of Barrier Heights for Heavy Atom Transfer, Nucleophilic Substitution, Association, and Unimolecular Reactions and Its Use to Test Theoretical Methods. *J. Phys. Chem. A* **2005**, *109*, 2012–2018.
- (40) Zhao, Y.; Lynch, B. J.; Truhlar, D. G. Development and Assessment of A New Hybrid Density Functional Model for Thermochemical Kinetic. *J. Phys. Chem. A* **2004**, *108*, 2715–2719.
- (41) Zhao, Y.; Truhlar, D. G. Hybrid Meta Density Functional Theory Methods for Thermochemistry, Thermochemical Kinetics, and Noncovalent Interactions: The MPW1B95 and MPWB1K Models and Comparative Assessment for Hydrogen Bonding and Van der Waals Interactions. *J. Phys. Chem. A* **2004**, *108*, 6908–6918.
- (42) Zhao, Y.; Schultz, N. E.; Truhlar, D. G. Design of Density Functionals by Combining the Method of Constraint Satisfaction with Parametrization for Thermochemistry, Thermochemical Kinetics, and Noncovalent Interactions. *J. Chem. Theory Comput.* **2006**, *2*, 364–382.
- (43) Zhao, Y.; Truhlar, D. G. The M06 Suite of Density Functionals for Main Group Thermochemistry, Thermochemical Kinetics, Non-Covalent Interactions, Excited States, and Transition Elements: Two New Functionals and Systematic Testing of Four M06-Class Functionals and 12 Other Functionals. *Theor. Chem. Acc.* **2008**, *120*, 215–241.

- (44) Boese, A. D.; Martin, J. M. L. Development of Density Functionals for Thermochemical Kinetics. *J. Chem. Phys.* **2004**, *121*, 3405–3416.
- (45) Chai, J. D.; Head-Gordon, M. Systematic Optimization of Long-Range Corrected Hybrid Density Functionals. *J. Chem. Phys.* **2008**, *128*, 084106.
- (46) Yanai, T.; Tew, D.; Handy, N. C. A New Hybrid Exchange-Correlation Functional Using the Coulomb-Attenuating Method (CAM-B3LYP). *Chem. Phys. Lett.* **2004**, *393*, 51–57.
- (47) Chai, J. D.; Head-Gordon, M. Long-Range Corrected Hybrid Density Functionals with Damped Atom-Atom Dispersion Corrections. *Phys. Chem. Chem. Phys.* **2008**, *10*, 6615–6620.
- (48) Adamo, C.; Barone, V. Exchange Functionals with Improved Long-Range Behavior and Adiabatic Connection Methods without Adjustable Parameters: The mPW and mPW1PW Models. *J. Chem. Phys.* **1998**, *108*, 664–675.
- (49) Perdew, J. P.; Wang, Y. Accurate and Simple Analytic Representation of the Electron-Gas Correlation Energy. *Phys. Rev. B: Condens. Matter Mater. Phys.* **1992**, *45*, 13244–13249.
- (50) Zhao, Y.; Schultz, N. E.; Truhlar, D. G. Exchange-Correlation Functional with Broad Accuracy for Metallic and Nonmetallic Compounds, Kinetics, and Noncovalent Interactions. *J. Chem. Phys.* **2005**, *123*, 161103.
- (51) Perdew, J. P.; Burke, K.; Ernzerhof, M. Generalized Gradient Approximation Made Simple. *Phys. Rev. Lett.* **1996**, *77*, 3865–3868.
- (52) Perdew, J. P.; Burke, K.; Ernzerhof, M. Errata: Generalized Gradient Approximation Made Simple [Phys. Rev. Lett. *77*, 3865 (1996)]. *Phys. Rev. Lett.* **1997**, *78*, 1396–1396.
- (53) Adamo, C.; Barone, V. Toward Reliable Density Functional Methods without Adjustable Parameters: the PBE0 Model. *J. Chem. Phys.* **1999**, *110*, 6158–6170.
- (54) Becke, A. D. Density-Functional Thermochemistry. III. The Role of Exact Exchange. *J. Chem. Phys.* **1993**, *98*, 5648–5652.

- (55) Heyd, J.; Scuseria, G. E. Efficient Hybrid Density Functional Calculations in Solids: Assessment of the Heyd-Scuseria-Ernzerhof Screened Coulomb Hybrid Functional. *J. Chem. Phys.* **2004**, *121*, 1187–1192.
- (56) Heyd, J.; Scuseria, G. E. Assessment and Validation of a Screened Coulomb Hybrid Density Functional. *J. Chem. Phys.* **2004**, *120*, 7274–7280.
- (57) Heyd, J.; Peralta, J. E.; Scuseria, G. E.; Martin, R. L. Energy Band Gaps and Lattice Parameters Evaluated with the Heyd-Scuseria-Ernzerhof Screened Hybrid Functional. *J. Chem. Phys.* **2005**, *123*, 174101.
- (58) Heyd, J.; Scuseria, G. E.; Ernzerhof, M. Erratum: "Hybrid Functionals Based on A Screened Coulomb Potential" [J. Chem. Phys. 118, 8207 (2003)] *J. Chem. Phys.* **2006**, *124*, 219906.
- (59) Izmaylov, A. F.; Scuseria, G.; Frisch, M. J. Efficient Evaluation of Short-Range Hartree-Fock Exchange in Large Molecules and Periodic Systems. *J. Chem. Phys.* **2006**, *125*, 104103.
- (60) Krukau, A. V.; Vydrov, O. A.; Izmaylov, A. F.; Scuseria, G. E. Influence of the Exchange Screening Parameter on the Performance of Screened Hybrid Functionals. *J. Chem. Phys.* **2006**, *125*, 224106.
- (61) Henderson, T. M.; Izmaylov, A. F.; Scalmani, G.; Scuseria, G. E. Can Short-Range Hybrids Describe Long-Range-Dependent Properties? *J. Chem. Phys.* **2009**, *131*, 044108.
- (62) Schmider, H. L.; Becke, A. D. Optimized Density Functionals from the Extended G2 Test Set. *J. Chem. Phys.* **1998**, *108*, 9624–9631.
- (63) Tao, J. M.; Perdew, J. P.; Staroverov, V. N.; Scuseria, G. E. Climbing the Density Functional Ladder: Nonempirical Meta-Generalized Gradient Approximation Designed for Molecules and Solids. *Phys. Rev. Lett.* **2003**, *91*, 146401.
- (64) Zhao, Y.; Lynch, B. J.; Truhlar, D. G. Multi-Coefficient Extrapolated Density Functional Theory for Thermochemistry and Thermochemical Kinetics. *Phys. Chem. Chem. Phys.* **2005**, *7*, 43–52.

- (65) Zhao, Y.; Truhlar, D. G. A New Local Density Functional for Main-Group Thermochemistry, Transition Metal Bonding, Thermochemical Kinetics, and Noncovalent Interactions. *J. Chem. Phys.* **2006**, *125*, 194101.
- (66) Van Voorhis, T.; Scuseria, G. E. A Novel Form for the Exchange-Correlation Energy Functional. *J. Chem. Phys.* **1998**, *109*, 400–410.
- (67) Lee, C.; Yang, W.; Parr, R. G. Development of the Colle-Salvetti Correlation-Energy Formula into a Functional of the Electron Density. *Phys. Rev. B: Condens. Matter Mater. Phys.* **1988**, *37*, 785–789.
- (68) Becke, A. D. Density-Functional Exchange-Energy Approximation with Correct Asymptotic Behavior. *Phys. Rev. A: At., Mol., Opt. Phys.* **1988**, *38*, 3098–3100.
- (69) Perdew, J. P. Density-Functional Approximation for the Correlation Energy of the Inhomogeneous Electron Gas. *Phys. Rev. B: Condens. Matter Mater. Phys.* **1986**, *33*, 8822–8824.
- (70) Lau, K.-C.; Ng, C.-Y. Benchmarking State-of-the-Art ab Initio Thermochemical Predictions with Accurate Pulsed-Field Ionization Photoion-Photoelectron Measurements. *Acc. Chem. Res.* **2006**, *39*, 823–829.
- (71) Shiell, R. C.; Hu, X. K.; Hu, Q. J.; Hepburn, J. W. A Determination of the Bond Dissociation Energy ($D_0(\text{H-SH})$): Threshold Ion-Pair Production Spectroscopy (TIPPS) of a Triatomic Molecule. *J. Phys. Chem. A* **2000**, *104*, 4339–4342.
- (72) Gibson, S. T.; Greene, J. P.; Berkowitz, J. A Photoionization Study of SeH and H₂Se. *J. Chem. Phys.* **1986**, *85*, 4815–4824.
- (73) Underwood, J.; Chastaing, D.; Lee, S.; Wittig, C. Heavy Hydrides: H₂Te Ultraviolet Photochemistry. *J. Chem. Phys.* **2005**, *123*, 084312.